Systems & Control Transactions

Research Article - Peer Reviewed Conference Proceeding
ESCAPE 35 - European Symposium on Computer Aided Process Engineering
Ghent, Belgium. 6-9 July 2025
Jan F.M. Van Impe, Grégoire Léonard, Satyajeet S. Bhonsale,
Monika E. Polańska, Filip Logist (Eds.)

PSE PRESS

Process Design of an Industrial Crystallization Based on Degree of Agglomeration

Yung Shun Kang[a], Hemalatha Kilari[a], Neda Nazemifard[b], Ben Renner[b], Yihui Yang[b], Charles Papageorgiou[b], and Zoltan K. Nagy[a]*

[a] Purdue University, Davidson School of Chemical Engineering, West Lafayette, Indiana, United States
[b] Takeda Pharmaceuticals International Company, Cambridge, Massachusetts, United States
* Corresponding Author: zknagy@purdue.edu

ABSTRACT

This study proposes a model-based approach utilizing a hybrid population balance model (PBM) to optimize temperature profiles for minimizing agglomeration and enhancing crystal growth. The PBM incorporates key mechanisms—nucleation, growth, dissolution, agglomeration, and deagglomeration—and is applied to the crystallization of an industrial active pharmaceutical ingredient (API), Compound K. Parameters were estimated through prior design of experiments (DoE) and refined via additional thermocycle experiments. In-silico DoE simulations demonstrate that the hybrid PBM outperforms traditional methods in assessing process performance under agglomeration-prone conditions. Results confirm that thermocycles effectively reduce agglomeration and promote bulk crystal formation, though their efficiency plateaus beyond a certain cycle number. This model-based approach provides a more robust strategy for agglomeration control compared to conventional methods, offering valuable insights for industrial crystallization optimization.

Keywords: Algorithms, Batch Process, Modelling and Simulations, Process Design, Optimization

1. INTRODUCTION

Agglomeration, often undesirable in crystallization, can lead to impurity incorporation [1,2], prolonged filtration and drying times, and difficulties in achieving uniform particle size and composition. While controlling supersaturation and agitation rates has been shown to reduce agglomeration [1,3], more advanced techniques, such as thermocycles, can facilitate deagglomeration and dissolve fines generated by breakage or attrition.

Optimizing thermocycles requires determining key parameters such as the number of heating-cooling cycles and the corresponding rates. This presents a complex optimization challenge, as traditional quality-by-control (QbC) methods relying on process analytical technology can be resource-intensive [4,5]. A more efficient alternative is the use of PBMs to monitor and regulate agglomeration during crystallization [6].

In this study, we propose a model-based approach to optimize temperature profiles for minimizing agglomeration and enhancing crystal size. A PBM is coupled with the number density of agglomerates to track agglomeration dynamics during thermocycles. The hybrid PBM incorporates key mechanisms, including nucleation, growth, dissolution, agglomeration, and deagglomeration, and is applied to the crystallization of an industrial active pharmaceutical ingredient, Compound K. Most parameters were estimated through DoE in a prior study, while additional thermocycle experiments were conducted to refine dissolution parameters.

Results from in-silico DoE simulations demonstrate that the hybrid PBM approach outperforms traditional methods in accurately evaluating process performance when agglomeration is present. This approach offers a more robust assessment of agglomeration control compared to methods based solely on particle bridge formation. Moreover, simulations indicate that while thermocycles effectively reduce agglomeration, their efficiency plateaus after a certain number of cycles—a trend confirmed through experiments in industrial case studies. Additionally, comparisons of different temperature profiles reveal that introducing heating-cooling cycles not only eliminates most agglomerates but also promotes the growth of larger bulk crystals.

The remainder of this article is organized as follows. Section 2 describes the experimental setup and measurement procedures. Using the experimental data, thermodynamic expressions and related parameters are defined for simulating the industrial case study. Section 3 introduces the hybrid PBMs, which are explicitly formulated to describe total number density and agglomerate number density under both heating and cooling conditions. Section 4 presents the results, including comparisons of different algorithms for agglomeration assessment and various optimal temperature trajectories. Additionally, it examines the differences between model-free and model-based QbC approaches in the industrial case study. Finally, conclusions are summarized in the last section.

2. MATERIALS, MEASUREMENTS, AND PROPOSED METHODOLOGY

2.1 Experimental setup and procedure

Batch experiments were conducted using the advanced synthesis workstation, Mettler Toledo's EasyMax 402, equipped with a 100 mL glass vessel. The vessel was sealed with a polytetrafluoroethylene lid, which provided multiple ports for PAT tools. Temperature control was achieved using a Pt100 temperature sensor and a Peltier plate, regulated by the built-in software, iControl. The process temperature was maintained between 0 and 70 °C to optimize yield while minimizing solvent evaporation.

Solvent selection for crystallization was performed through a solvent screening process. The chosen mixture consisted of dimethyl sulfoxide (DMSO, 100%, Fisher Scientific) and ethanol (EtOH, 100% absolute, Decon Laboratories, Inc.) in a volume ratio of 20:80. The industrial compound used in this study, referred to as Compound K and supplied by Takeda, exhibited a wide metastable zone—a topic explored in detail in the results section. This broad metastable zone prevented precipitation or nucleation at high supersaturation levels, allowing for a higher initial concentration to enhance productivity and yield.

Due to Compound K's poor solubility in EtOH (forming needle-like but highly agglomerated particles), it was initially dissolved in DMSO. EtOH was then introduced as an antisolvent to control the solubility of the mixture. To ensure the solid form of the final product, a tailored seeding strategy was developed for the seeded batch experiments. Wet seeding was employed to prevent particle clumping and seed aggregation. The seed suspension was prepared in EtOH and sonicated using an ultrasonic cleaner (ELMA ULTRASONICS P30H). The total solvent volume was maintained at 100 mL, with solvent evaporation carefully monitored and typically kept below 5% of the total volume.

During the experiments, an upward-pitched blade metal agitator operated at 400 rpm to ensure efficient mixing. In situ microscopy was performed using Mettler Toledo's EasyViewer with iC Vision software to capture inline particle images and monitor key process mechanisms, including nucleation, growth, dissolution, and agglomeration. Solute concentration was measured using attenuated total reflectance Fourier transform infrared spectroscopy (ATR-FTIR) with Mettler Toledo's ReactIR 702L, following probe calibration.

To constrain the design space, the seed's origin was restricted to a specific lot from the company. The seed crystals were generated using the aforementioned solvent system, resulting in needle-like particles with a crystal size distribution characterized by D10, D50, and D90 values of 2.51, 9.06, and 20.5 μm, respectively. Differential scanning calorimetry (DSC) measurements revealed that the seed was partially crystalline, with a crystallinity of 54.4%.

2.2 Crystal size distribution measurement

In the experimental analysis of solid samples, the crystal size distribution (CSD) was determined using the Mastersizer 3000, a Malvern instrument that utilizes light scattering. For wet measurements, heptane (100%, Fisher Scientific) with a fixed amount of Span 80 (100%, Fisher Scientific) was used as the dispersant. Prior to measurement, the slurry was sonicated at 20% intensity for 60 seconds to ensure effective dispersion.

2.3 Crystallinity measurement

Qualitative analyses were conducted to assess potential changes in the solid form during the experimental process using offline techniques such as X-ray Powder Diffraction (XRD). These methods were employed to identify distinctive features or fingerprints of the materials. Given the small particle size, scanning electron microscopy (SEM) images of the final products were captured using a field-emission SEM (FEI Nova NanoSEM 450) to confirm the crystal habit and evaluate the extent of agglomeration.

DSC was deemed essential in this study due to the presence of amorphous content, a factor further discussed in the results section. DSC measurements were performed using a PerkinElmer Jade DSC instrument. Notably, the primary purpose of DSC in this study was to enable quantitative comparisons rather than to determine precise thermodynamic properties. The melting heat was quantified based on the area under the melting peak, and crystallinity was calculated as the ratio of the melting heat of the sample to that of an established standard.

2.4 Solubility measurement

Utilizing the UPLC data, a crystalline solubility curve was constructed employing the following empirical

equation:

$$ln(C_{s,cry}) = a + \frac{b}{R*T} + \frac{c}{(R*T)^2} \quad (1)$$

where $C_{s,cry}$ represents the crystalline solubility with the unit of mg/g solvent, T denotes the temperature in Kelvin, and R stands for the ideal gas constant. The coefficients' values in the solubility equation are provided in Table 1.

Table 1: The solubility coefficients of Compound K in crystalline form.

Coefficient	Value	Unit
a	44.84	-
b	1.891×10^5	$J{\cdot}mol^{-1}$
c	2.016×10^8	$J^2{\cdot}mol^{-2}$

Table 2: The solubility coefficients of Compound K in amorphous form.

Coefficient	Value	Unit
a	−98.06	-
b	1383	K
c	16.73	-

Following the identification of the amorphous form, the solubility data for the amorphous phase was collected and fitted using Equation 2. The parameters of the solubility curve for the amorphous form are presented in Table 2.

$$ln(C_{s,amor}) = a + \frac{b}{T} + c * log(T) \quad (2)$$

where $C_{s,amor}$ represents the amorphous solubility with the unit of mg/g solvent.

Table 3: The boundaries of shape descriptors for different classes of particles.

Classes	*L	*I	*A	*C
Droplets	-	> 100	-	> 0.87
Needles	>2.0	< 100	> 0.32	< 0.87
agglomerates	>2.0	< 100	< 0.32	< 0.87
Fines	<2.0	< 100	-	< 0.87

* L: Length, I: Intensity Mean, A: Aspect ratio, C: Circularity

2.5 Degree of agglomeration measurement

To analyze the degree of agglomeration and ensure proper dispersion of the highly agglomerated final particles, the solid sample was suspended in the same dispersant used for the CSD measurement. The solid content concentration was controlled at approximately 0.7 mg/mL to prevent excessive particle overlap under the microscope. After sonication, the slurry was uniformly applied to the measurement slide, which was then dried under air.

The Morphologi 4 was used to conduct the image analysis on the prepared slide. Based on various shape descriptors, the particles were classified into four categories: fines, needles, agglomerates, and droplets, as

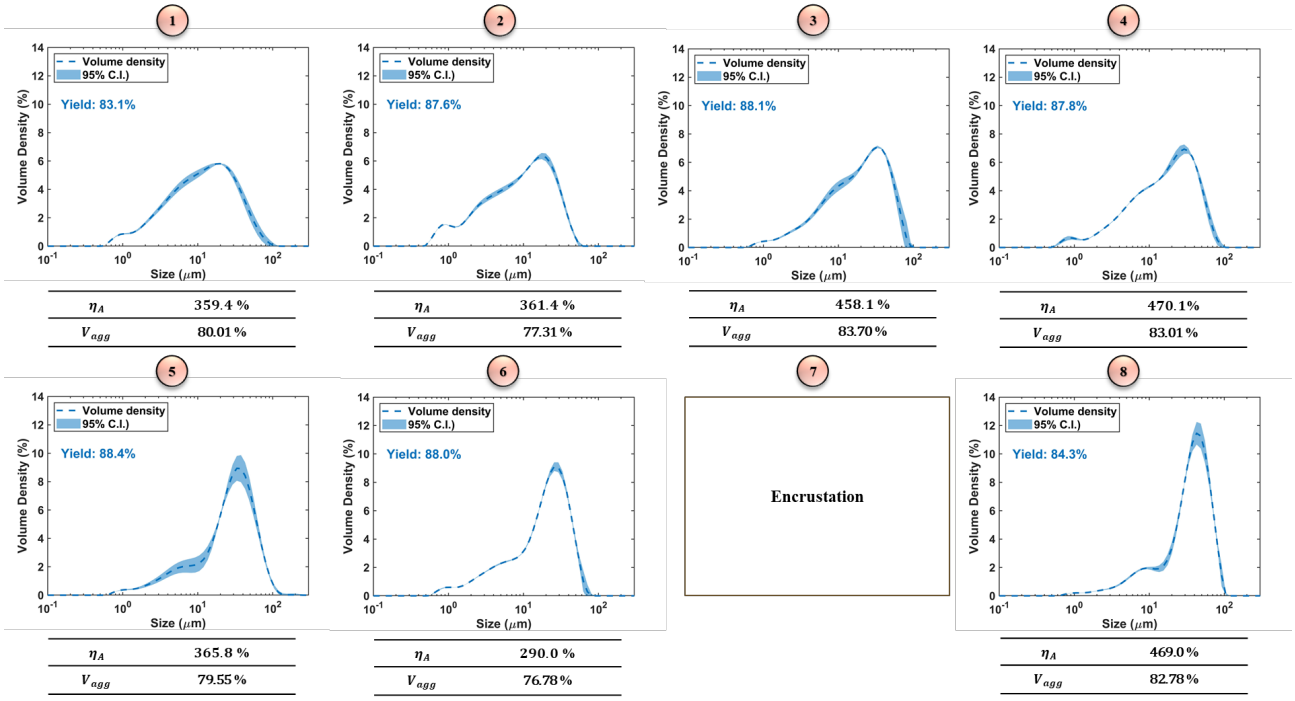

Figure 1: Degree of agglomeration calculation comparison based on the in-silico DoE study.

shown in Table 3. The degree of agglomeration was calculated by determining the percentage fraction of agglomerates, needles, and fines, while droplets were excluded due to their role as surfactants for particle dispersion. A minimum of 100,000 particles were captured during the analysis, ensuring that the calculated values represent the overall distribution. The remaining image analysis settings are shown in Supplemental Materials.

3. DEGREE OF AGGLOMERATION POPULATION BALANCE MODELING IN INDUSTRIAL CRYSTALLIZATION

Previous trial experiments have shown that the concentration trajectory intersects the amorphous solubility curve throughout heating and cooling cycles. This observation highlights a key aspect of the thermocycling process: the limited dissolution of crystalline particles, even during rapid heating. This behavior supports the continuous growth of needle-like particles across the thermocycles, leading to their eventual enlargement. Consequently, for the digital design of the process, aimed at capturing the evolution of both crystalline and amorphous materials during the desaturation phase, as well as the dissolution behavior of amorphous materials during heating, the degree of supersaturation is defined as follows:

$$\begin{cases} \sigma = \frac{C - C_{s,cry}}{C_{s,cry}}, & C > C_{s,amor} \\ \sigma = \frac{C - C_{s,amor}}{C_{s,amor}}, & C < C_{s,amor} \end{cases} \tag{3}$$

where σ denotes the degree of supersaturation, $C_{s,cry}$ denotes the crystalline solubility, $C_{s,amor}$ denotes the crystalline solubility, and C represents the solution concentration.

$$\frac{\partial f(L,t)}{\partial t} + g(t;\theta_g)\frac{\partial f(L,t)}{\partial L} = B_n(t;\theta_n)\delta(L - L_n) - f(L)\int_0^L \beta(L,\lambda)f(\lambda)d\lambda + \frac{L^2}{2}\int_0^\infty \frac{\beta\left((L^3 - \lambda^3)^{\frac{1}{3}},\lambda\right)}{(L^3 - \lambda^3)^{\frac{2}{3}}} f\left((L^3 - \lambda^3)^{\frac{1}{3}}\right) f(\lambda)d\lambda$$

$$while\ C > C_{s,amor} \tag{4}$$

The 1D PBM for this thermocycling process is expressed in equations (4) and (5). These equations are presented in two stages: the heating stage, which results in an undersaturated region, and the cooling stage, which leads to a supersaturated region.

$$\frac{\partial f(L,t)}{\partial t} - D(t;\theta_d)\frac{\partial f(L,t)}{\partial L} = -S(L)f(L,t)\int_\lambda^{L_{max}} b(L,\lambda)S(\lambda)f(\lambda,t)d\lambda$$

$$while\ C < C_{s,amor} \tag{5}$$

where f is the number density function of the total number density, g is the growth rate of the agglomerates with the corresponding parameters θ_g, d is the dissolution rate with the corresponding parameters θ_d, B_n is the birth of the particles due to the nucleation, β and b are agglomeration and breakage kernels. $b(L,\lambda)$ is defined as the inverse function of size-dependent Brownian collision kernel to capture the deagglomeration mechanism. $S(L)$ is the selection function for the deagglomeration process, which is a size-independent function:

$$S(L) = k_{dg}D^{g_d} \tag{6}$$

To monitor the evolution of agglomeration during thermal cycles, the PBM for agglomerate number density is coupled with the PBM for total number density, as represented by equations (7) and (8), formulated as follows:

$$\frac{\partial f_{agg}(L,t)}{\partial t} + g_{agg}(t;\theta_g)\frac{\partial f_{agg}(L,t)}{\partial L} = -f(L)\int_0^L \beta(L,\lambda)f(\lambda)d\lambda + \frac{L^2}{2}\int_0^\infty \frac{\beta\left((L^3 - \lambda^3)^{1/3},\lambda\right)}{(L^3 - \lambda^3)^{2/3}} f((L^3 - \lambda^3)^{1/3})f(\lambda)d\lambda$$

$$while\ C > C_{s,amor} \tag{7}$$

$$\frac{\partial f_{agg}(L,t)}{\partial t} - d_{agg}(t;\theta_d)\frac{\partial f_{agg}(L,t)}{\partial L} = -S(L)f(L,t) + \int_\lambda^{L_{max}} b(L,\lambda)S(\lambda)f(\lambda,t)d\lambda$$

$$while\ C < C_{s,amor} \tag{8}$$

The boundary conditions of f_{agg} are defined in equation (9), to ensure that the newly formed crystals are not classified as agglomerates and to ensure that the number of agglomerates never exceeds the total number of particles.

$$\begin{cases} \lim_{L\to 0} f_{agg}(L,t) = 0 \\ 0 \le \frac{f_{agg}(L,t)}{f(L,t)} \le 1 \end{cases} \tag{9}$$

To quantify the degree of agglomeration of the particles, a volume-based degree of agglomeration (V_{agg}) is defined as follow:

$$V_{agg} = \frac{\int_0^\infty f_{agg}(L,t)L^3 dL}{\int_0^\infty f(L,t)L^3 dL} \tag{10}$$

In addition to the degree of agglomeration defined

earlier, an alternative method for estimating agglomeration is also employed in this work. According to the literature, the degree of agglomeration (η_A) is determined by the ratio of the "number of bridges" (N_A) to the total number of particles. By monitoring the formation and breakage of bridges during the process, the number of agglomeration bridges per unit volume of suspension is calculated. A detailed derivation of this method is provided in [6].

Finally, the PBMs are closed by the mass balance equations given by

$$\frac{dC(t)}{dt} = -k_v \rho_c \left[3G(t;\theta_g) \int_0^\infty L^2 f(L) dL + B(t;\theta_b) L_n^3 \right]$$

$$while\ C > C_{s,amor} \tag{11}$$

$$\frac{dC(t)}{dt} = 3k_v \rho_c \left[D \int_0^\infty L^2 f(L) dL \right]$$

$$while\ C < C_{s,amor} \tag{12}$$

Where $k_v$is the volume shape factor of the crystals, ρ_c is the crystal density, and D represents the dissolution kinetics, which is formulated as follow:

$$D = k_d \sigma \tag{13}$$

The kinetics parameters are shown in Supplemental Materials (LAPSE:2025.0037), which most of them are directly obtained from the iterative model-based experimental design framework [7]. (Dissolution and deagglomeration kinetics are estimated with a simple factorial DoE, since their formulations are much simpler compared with those mechanisms during the desaturation.)

4. RESULT AND DISCUSSIONS

To assess the degree of agglomeration using this hybrid PBM framework, an in-silico case study was conducted by replicating the experimental conditions detailed in the DoE shown in Supplemental Materials, with variations in the decision variables. As illustrated in Figure 1, the degree of agglomeration derived from the hybrid PBM framework offers a more accurate estimation compared to the agglomerate degree based solely on the number of bridges. This improvement stems from the fact that within the agglomerates, there exists a considerable probability of multiple bridges forming, rendering a simple bridge count an overestimation of the degree of agglomeration.

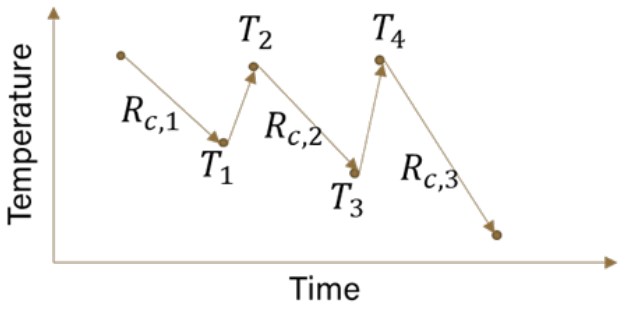

Figure 2: Input features that were used to describe the thermocyclic temperature profiles.

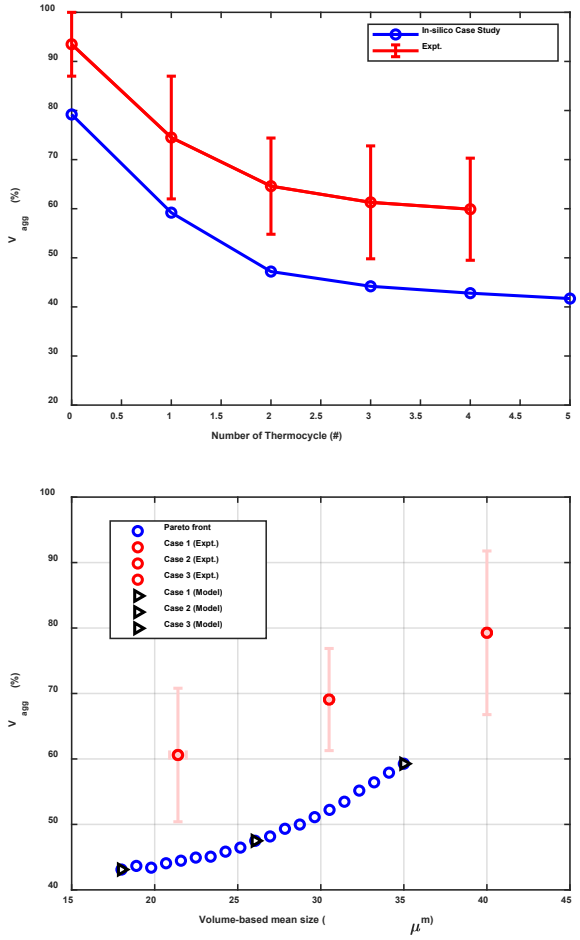

Figure 3: The comparison between V_{agg}.and different number of thermocycles (Top). The comparison between V_{agg}.and particle size while varying weighting factors in the optimization (N = 3) (Bottom).

In essence, the application of the degree of agglomeration derived from this hybrid framework presents a more comprehensive approach than prior methodologies. However, it is noteworthy that as the model was not trained using the degree of agglomeration from experimental results, there remains room for enhancing the predictive capacity of the model in future iterations.

Linear cooling 0.05 °C/min

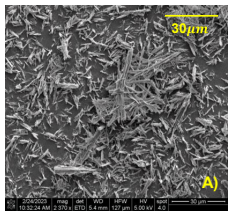

Cumulative CSD	D10	D50	D90
Unit (μm)	1.84	13.1	38.8
Crystallinity	43.9% ± 7.3%		
Yield	90.8% ± 0.5%		
V_{Agg} (Model)	79.2%		
V_{Agg} (Expt.)	96.8% ± 12.4%		
Batch time (hr)	14		
Solute Dissolved	~46.3 mg/ml solvent		
Seed loading	5%		

Three-cycle TDNC profile

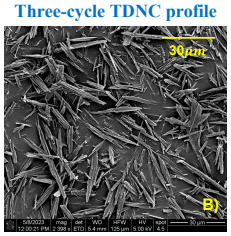

Cumulative CSD	D10	D50	D90
Unit (μm)	2.8	17.0	50.0
Crystallinity	83.3% ± 7.2%		
Yield	93.6% ± 0.2%		
V_{Agg} (Model)	46.0%		
V_{Agg} (Expt.)	56.7% ± 15.6%		
Batch time (hr)	46		
Solute Dissolved	~46.3 mg/ml solvent		
Seed loading	5%		

Two-cycle optimal profile

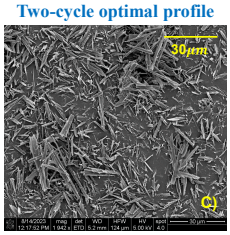

Cumulative CSD	D10	D50	D90
Unit (μm)	2.2	16.8	39.2
Crystallinity	75.6% ± 5.7%		
Yield	92.6% ± 0.7%		
V_{Agg} (Model)	44.2%		
V_{Agg} (Expt.)	64.6% ± 15.4%		
Batch time (hr)	20		
Solute Dissolved	~46.3 mg/ml solvent		
Seed loading	5%		

Three-cycle optimal profile

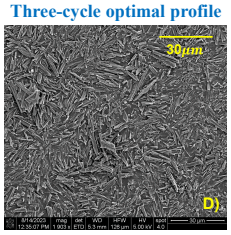

Cumulative CSD	D10	D50	D90
Unit (μm)	2.0	10.8	38.0
Crystallinity	78.6% ± 8.7%		
Yield	91.6% ± 0.5%		
V_{Agg} (Model)	42.8%		
V_{Agg} (Expt.)	61.3% ± 12.3%		
Batch time (hr)	25		
Solute Dissolved	~46.3 mg/ml solvent		
Seed loading	5%		

Figure 4: Experimental summaries of the linear cooling profile, the model-free QbC profile and the optimal

To reduce the degree of agglomeration of the final product, an optimization was formulated for a seeded crystallization. The decision variables are the 2N discrete temperature values that define the temperature profile as shown in Figure 2. The optimization objectives were to determine the temperature profile that minimizes the degree of agglomeration throughout the process and increase the size of the fine particles. For this, the following objective function was used:

$$\min_{\gamma \in R} OF = \omega V_{agg} + (1-\omega)\frac{1}{(\mu_1/\mu_0)}$$

$$\gamma = (R_{c,j}, T_j) \tag{14}$$

where $R_{c,j}$ is the cooling rate of each segment ($j = N+1$), T_j are the temperature turning points ($j = 2N$), and N denotes the number of thermocycles. (μ_1/μ_0) represents the number-based mean size of the final products.

Various optimal temperature profiles were generated, as shown in Figure 3. As the number of thermocycles increases, V_{agg} gradually decreases and eventually reaches a plateau. This trend is consistent in both the in-silico study and experimental results. By adjusting the weighting factors, the model demonstrates a similar trend to the experimental validations, despite an offset attributed to the model's limited accuracy in predicting the exact value of V_{agg}.

Figure 4 presents an experimental comparison of the linear cooling profiles, the model-free QbC profile—developed using a turbidity-based direct nucleation control strategy, which indirectly regulates fine particle generation and promotes seed particle growth—and the optimal temperature profiles obtained from the optimization problem discussed earlier. The results indicate that optimal temperature profiles perform comparably to the model-free QbC profile and outperform linear cooling profiles in terms of reducing the degree of agglomeration, not to mention the improvement in crystallinity. Additionally, they offer significant advantages by shortening batch time. (The optimal temperature profiles suggest that batch time could be further reduced by increasing cooling rates during the thermal cycle without compromising the degree of agglomeration.) This improvement in agglomeration has been validated through image analysis using Morphologi 4, based on the number-based degree of agglomeration analysis (N_{agg}) and SEM images.

5. CONCLUSION

This study demonstrates the effectiveness of a model-based approach using a hybrid population balance model (PBM) to optimize temperature profiles for industrial crystallization processes. The hybrid PBM, which integrates critical mechanisms such as nucleation, growth, dissolution, agglomeration, and deagglomeration, provides a more accurate and comprehensive framework for minimizing agglomeration and promoting crystal growth than traditional methods.

The in-silico design of experiments (DoE) simulations and experimental validations confirmed that optimal temperature profiles and thermocycles significantly reduce the degree of agglomeration and enhance bulk crystal formation. While thermocycles proved effective, their benefits plateau with an increasing number of cycles. Additionally, the optimal temperature profiles outperformed linear cooling strategies in both reducing agglomeration and shortening batch times, demonstrating scalability and efficiency for industrial applications.

By integrating insights from image analysis (Morphologi 4 and SEM) and validating findings through experimental data, this study demonstrates how model-based optimization enhances both process control and product quality. Future research may focus on improving model accuracy by incorporating agglomeration data from experimental results to further refine predictive capabilities. Ultimately, this approach provides a robust and

scalable strategy for crystallization optimization, offering valuable insights while effectively managing the degree of agglomeration in the pharmaceutical and specialty chemical industries. Additionally, the hybrid PBM structure has shown significant potential for application in granulation and spherical agglomeration processes, facilitating improved control over particle formulation related to aggregation and agglomeration.

ACKNOWLEDGEMENTS

This academic project was funded by Takeda Pharmaceuticals.

REFERENCES

1. Urwin, Stephanie J., et al. "A structured approach to cope with impurities during industrial crystallization development." Organic process research & development 24.8 (2020): 1443-1456.
2. Terdenge, Lisa-Marie, and Kerstin Wohlgemuth. "Impact of agglomeration on crystalline product quality within the crystallization process chain." *Crystal Research and Technology* 51.9 (2016): 513-523.
3. Sun, Zhuang, et al. "Use of Wet Milling Combined with Temperature Cycling to Minimize Crystal Agglomeration in a Sequential Antisolvent–Cooling Crystallization." *Crystal Growth & Design* 22.8 (2022): 4730-4744.
4. Fujiwara, Mitsuko, et al. "First-principles and direct design approaches for the control of pharmaceutical crystallization." *Journal of Process Control* 15.5 (2005): 493-504.
5. Wu, Wei-Lee, et al. "Implementation and application of image analysis-based turbidity direct nucleation control for rapid agrochemical crystallization process design and scale-up." *Industrial & Engineering Chemistry Research* 61.39 (2022): 14561-14572.
6. Szilagyi, Botond, et al. "Application of model-free and model-based quality-by-control (QbC) for the efficient design of pharmaceutical crystallization processes." *Crystal Growth & Design* 20.6 (2020): 3979-3996.
7. Kilari, Hemalatha, et al. "A Systematic Model Development Framework for Batch Crystallization Using Iterative Model-Based Experimental Design Approach." *2023 AIChE Annual Meeting*. AIChE, 2023.